Microscopic optical-model calculations of neutron total cross sections and cross section differences

H. S. Camarda
Penn State University, Delaware County Campus, Media, Pennsylvania 19063

F. S. Dietrich and T. W. Phillips
Lawrence Livermore National Laboratory, Livermore, California 94550
(Received 16 January 1989)

Using the microscopic optical model of Jeukenne, Lejeune, and Mahaux we have calculated the absolute neutron total cross sections and cross section differences of ^{140}Ce, ^{139}La–^{140}Ce, ^{141}Pr–^{140}Ce, ^{142}Ce–^{140}Ce, and ^{40}Ca, ^{44}Ca–^{40}Ca from 6–60 MeV and have made comparisons with experimental data. Except for ^{142}Ce–^{140}Ce, reasonable agreement with the mass 140 data was achieved with proton densities ρ_p of the nuclei determined by μ^- data and neutron densities determined by the relationship $\rho_n=(N/Z)\rho_p$ which implies $\Delta r_{np}=\langle r_n^2\rangle^{1/2}-\langle r_p^2\rangle^{1/2}=0$. Satisfactory agreement with the ^{142}Ce–^{140}Ce data was obtained by choosing a ρ_n for ^{142}Ce with $\Delta r_{np}=0.05$ fm and by a 10% increase in the strength of the ^{142}Ce imaginary potential. Similar choices of Δr_{np} and imaginary potential strength were made for ^{44}Ca in trying to fit the ^{44}Ca–^{40}Ca data. Previous phenomenological analyses carried out for this data are in qualitative agreement with our results, which imply that the addition of a few neutrons to a nucleus with a closed neutron shell yields a nucleus with a slightly thicker neutron skin and a larger neutron reaction cross section when compared to their closed shell isotopes.

I. INTRODUCTION

The high precision with which total neutron cross section differences can be measured offers the possibility of observing subtle structure effects in the comparison of neighboring nuclei. In two recent papers[1,2] data on total cross section differences between nuclei in the mass-140 and mass-40 regions were interpreted via a phenomenological spherical optical model. In principle, an optical potential based on the microscopic folding model should be a more appropriate tool for extracting structural information, since this formulation of the optical potential is more fundamental and possesses fewer free parameters. Specifically, the microscopic model relates the scattering to the nuclear density and an effective nucleon-nucleon interaction.

In the present work, we employ a microscopic optical model based on the work of Jeukenne, Lejeune, and Mahaux[3–5] (JLM) to analyze neutron total cross sections in the range 6–60 MeV on ^{140}Ce and ^{40}Ca, along with cross section differences for ^{139}La–^{140}Ce, ^{141}Pr– ^{140}Ce, ^{142}Ce– ^{140}Ce, and ^{44}Ca– ^{40}Ca. The JLM-based optical potential has been systematically tested against data on neutron-scattering angular distributions over wide ranges of energy and target mass,[6–8] and found to yield reasonable agreement. In the following, experimental data are first compared with calculations based on proton densities fixed by electron-scattering and muonic x-ray data, and the simple assumption that neutron densities are proportional to proton densities. Where appropriate, changes in either the densities or other parameter of the optical model that improve agreement with the experimental data are noted.

II. USE OF JLM POTENTIAL

Using Reid's hard core interaction, JLM have calculated an optical potential that a nucleon, with an energy $E<160$ MeV, would experience in infinite nuclear matter. This optical potential is a function of the energy of the nucleon and the density of the infinite nuclear medium. By assuming that the optical potential at a point in finite nucleus where the density ρ is the same as the potential in infinite nuclear matter with the same density ρ [the local density approximation, (LDA)] comparisons could be made with results obtained by fitting spherical phenomenological optical potentials to nucleon scattering data off finite nuclei. Using the LDA led to good agreement with experimentally derived quantities sensitive to the interior of the nucleus but, not surprisingly, gave less than satisfactory agreement with quantities, e.g., root mean square radii, which are more sensitive to the surface of the finite nucleus.[4] Consequently, JLM suggested an improved LDA approximation wherein the infinite nuclear matter potential is convoluted with a Gaussian smearing function with a range of ~ 1 fm. This smearing accounts in an approximate manner for the finite range of the effective interaction between the projectile and target nucleons. This procedure is somewhat arbitrary, and as pointed out in Ref. 6 the improved LDA can be represented more generally by

$$U(\mathbf{r},E)^{\mathrm{FN}}=\int \frac{U(\rho(\mathbf{r}''),E)^{\mathrm{NM}}}{\rho(\mathbf{r}'')}\rho(\mathbf{r}')f(\mathbf{r}-\mathbf{r}')d\mathbf{r}' , \quad (1)$$

where FN, NM refer to finite-nucleus and nuclear-matter optical potentials, ρ is the nuclear density (with isospin labels suppressed), and f is a Gaussian smearing function.

Various choices for $\mathbf{r}''$ are possible: The alternatives $\mathbf{r}''=\mathbf{r}'$ and $\mathbf{r}''=\mathbf{r}$ were suggested by JLM,[4] whereas $\mathbf{r}''=(\mathbf{r}+\mathbf{r}')/2$ was employed in the systematic survey of Refs. 6–8. The last choice is used in the present work except where noted otherwise. The differences among these prescriptions affect primarily the imaginary potential, which is strongly density dependent; examples are shown in Ref. 6.

We have also implemented a correction to the JLM potential, suggested by Negele and Yazaki[9] and Fantoni *et al.*,[10] that involves multiplying the imaginary potential (before smearing) by an effective mass factor [the k mass, Eq. (29) of Ref. 4].

Given the density dependent nuclear matter optical potential derived by JLM, the critical inputs for determining a spherical optical potential for a nucleus of interest are the point proton and neutron densities suitable for that nucleus. All of our point proton densities were calculated from Woods-Saxon parametrization of either e^- scattering or μ^- x-ray charge data[11,12] by deconvoluting the finite charge distribution of the proton. In selecting point neutron densities we tested several possibilities. In some cases, point neutron densities were chosen to be N/Z times the point proton density. For this N/Z scaling the difference in rms radii of the neutron and proton densities $\langle r_n^2\rangle^{1/2}-\langle r_p^2\rangle^{1/2}=\Delta r_{np}=0$. In other cases, neutron densities were chosen such that $\Delta r_{np}>0$.

In keeping with previous uses of the model,[6,7] the range t of the Gaussian smearing function for both the real and imaginary parts of the potential was chosen to be 1 fm. This parameter was never varied. Also, the spin-orbit potential used was the Elliot M3Y force which previously was found to reproduce elastic analyzing power data.[6]

The resulting optical potentials were used in a spherical optical-model program where the cross sections to be compared with experimental data were calculated. Additional freedom was allowed here in that the overall strengths of the real and imaginary parts of the optical potentials were varied through the energy independent normalization factors λ_v and λ_w. Thus the only freedom we allowed ourselves in fitting the data below was to vary the input neutron densities and the normalization factors.

III. MASS 140 REGION

An absolute neutron total cross section measurement, σ_t, of ^{140}Ce and neutron total cross section difference measurements, $\Delta\sigma_t$, on ^{139}La–^{140}Ce, ^{141}Pr–^{140}Ce, and ^{142}Ce–^{140}Ce have been carried out for incident neutron energies 3–60 MeV.[1] The first two of the difference measurements are sensitive to changes which occur when a single proton is subtracted from or added to the reference closed neutron shell nucleus ($N=82$) ^{140}Ce, while the last difference measurement probes changes due to the addition of two neutrons to the $N=82$ neutron core of ^{140}Ce.

This data was analyzed with several different spherical phenomenological optical potentials.[1] Our interest in this data is twofold: (1) As a test of the microscopic JLM optical model and (2) to explore whether or not different conclusions might arise between the microscopic and phenomenological analyses of the data.

The microscopic optical-model calculation for the ^{140}Ce absolute neutron total cross section started with proton point densities determined by μ^- x-ray charge data and neutron point densities determined by N/Z scaling ($\Delta r_{np}=0$). For the same input densities, the improved LDA, as represented by Eq. (1), was applied with $\mathbf{r}''=\mathbf{r}'$, $\mathbf{r}''=(\mathbf{r}+\mathbf{r}')/2$, and $\mathbf{r}''=\mathbf{r}$ which we refer to as methods *a*, *b*, and *c*, respectively. For all three cases the spherical optical-model calculations were performed with fixed values of the normalizing factors $\lambda_v=0.95$, $\lambda_w=0.80$. We note that the values of λ_v, λ_w are consistent with previous applications of the model[6,7] using prescription *b* and that, as shown in Fig. 1, the predicted cross sections reflect the general behavior of the data satisfactorily. In particular, the location of the maxima and minima are reproduced remarkably well and at the 15 MeV maximum the calculated cross section differs from experiment by only 5%. The dotted, solid, and dot-dashed curves refer to the LDA *a*, *b*, and *c* as described above. The solid line probably represents this data best but there is no significant difference among the "fits" to the data.

In order to calculate the $\Delta\sigma_T$ for ^{139}La–^{140}Ce, the ^{140}Ce parameters were held fixed and input point densities for ^{139}La were constructed from μ^- x-ray charge data and N/Z scaling. The μ^- charge data were represented by a two-parameter Fermi distribution with a constant diffuseness and a half-density radius which varied with the nucleus. All other adjustable parameters which entered the La calculation were the same as those for ^{140}Ce. Plotted in Fig. 2 are the fits to the ^{139}La–^{140}Ce difference

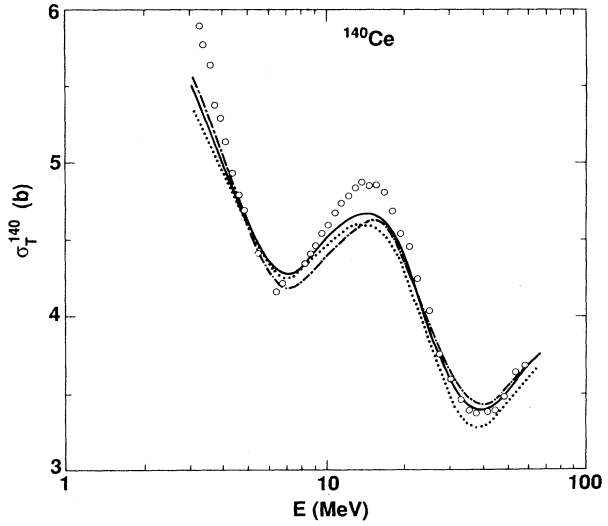

FIG. 1. The circles represent the measured ^{140}Ce neutron total cross section as a function of energy (Ref. 1). The dotted, solid, and dot-dashed curves represent the predictions of the microscopic model using the improved LDA *a*, *b*, and *c* as described in the text. The normalization constants for the real and imaginary parts of the potential are 0.95 and 0.80 for all three curves.

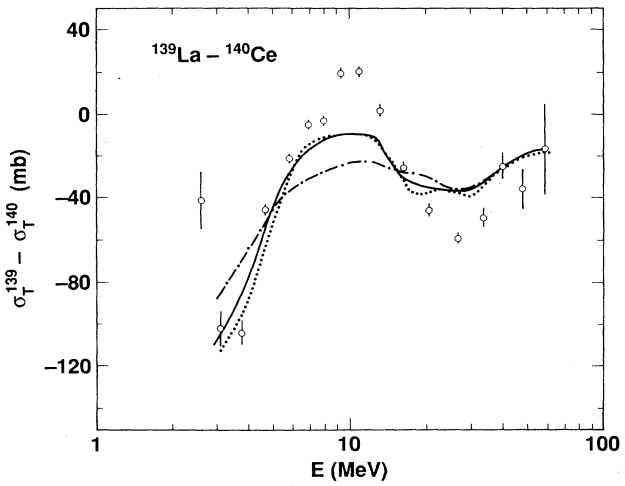

FIG. 2. The measured neutron total cross section difference of ^{139}La– ^{140}Ce as a function of energy (Ref. 1) is represented by the circles. The dotted, solid, and dot-dashed curves show the calculated cross section difference as a function of neutron energy as predicted by the microscopic optical model with the improved LDA *a*, *b*, and *c* described in the text.

data using the improved LDA *a*, *b*, and *c*. The predicted $\Delta\sigma_T$ for cases *a*, *b*, are indistinguishable and method *c* is somewhat less satisfactory than either *a* or *b*. Although the predicted oscillations of the data are somewhat muted, the overall behavior of the difference data is accounted for.

In all subsequent calculations the smearing of the infinite nuclear matter optical potential was carried out with $\mathbf{r}''=(\mathbf{r}+\mathbf{r}')/2$ (method *b*) in Eq. (1).

As for La, the ^{141}Pr σ_T calculation had input densities determined by μ^- x-ray data and N/Z scaling. The normalization constants λ_v, λ_w were chosen to have the

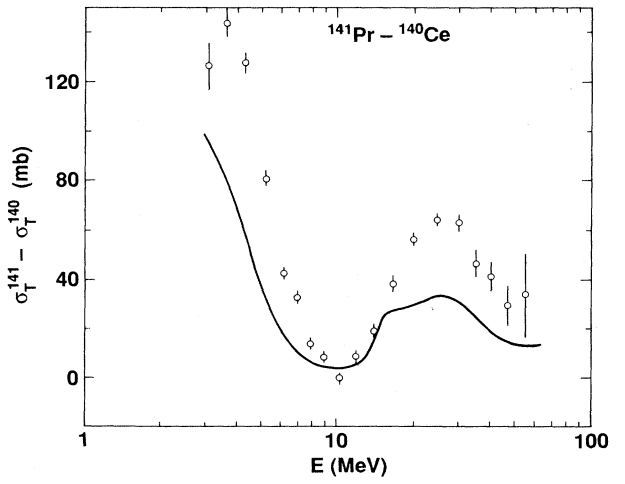

FIG. 3. The ^{141}Pr–^{140}Ce measured (circles) cross section of Ref. 1 and calculated (solid line) neutron total cross section difference.

^{140}Ce values of 0.95 and 0.80. The predicted ^{141}Pr–^{140}Ce $\Delta\sigma_T$ displayed in Fig. 3 agrees about as well with the data as that obtained for ^{139}La–^{140}Ce. Considering the small number of parameters which can be varied, the agreement between theory and experiment in these two cases is quite satisfactory.

The ^{142}Ce–^{140}Ce neutron $\Delta\sigma_T$ data represents a situation that differs from the previous two cases in that two neutrons are being added to the core nucleus ^{140}Ce and, in addition, adding the two neutrons to ^{140}Ce "breaks" the closed shell ($N=82$) structure.

Our first attempt at fitting the ^{142}Ce–^{140}Ce $\Delta\sigma_T$ data began as in the previous two cases by determining, for ^{142}Ce, proton and neutron densities with μ^- x-ray data and N/Z scaling and by choosing λ_v and λ_w to be 0.95 and 0.80. The results of this cross section difference calculation is the dotted line of Fig. 4. We note that the predicted $\Delta\sigma_T$ is qualitatively different than that determined for either La-Ce or Pr-Ce in that the calculated maxima and minima are out of phase with that of the data. By only changing λ_w from 0.80 to 0.88 we were able to significantly improve the fit (dot-dashed line of Fig. 4) above 4 MeV. Further improvement of the fit to the data was achieved by keeping the point proton density as before but by changing the neutron density so that $\Delta r_{np}=0.05$ fm. The input neutron density in this case was, initially, the smooth neutron distribution implied by N/Z scaling. This density was radially stretched (and renormalized) to yield the 0.05 fm difference in rms values. The calculation performed with these input densities for λ_v, λ_w equal to 0.95 and 0.88 yielded the solid line of Fig. 4. The fit to the data is quite good above 6 MeV. Taking

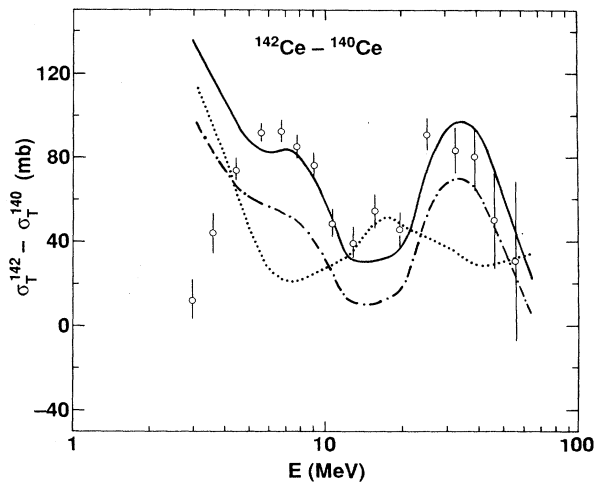

FIG. 4. Plotted are the measured (Ref. 1) and calculated $\Delta\sigma_T$ for ^{142}Ce–^{140}Ce as a function of neutron energy. The dotted curve represents a calculation in which the neutron density was N/Z times the proton density ($\Delta r_{np}=0$) and λ_v, λ_w are equal to 0.95, 0.80. The dot-dashed curve differs from the dotted one in that λ_w was increased from 0.80 to 0.88. The solid line represents the calculated $\Delta\sigma_T$ with $\Delta r_{np}=0.05$ fm and λ_v, λ_w equal to 0.95 and 0.88.

into consideration the 12 mb uncertainty of the experimental data, this analysis suggests that the *difference* of Δr_{np} in going from ^{140}Ce to ^{142}Ce is 0.05 ± 0.025 fm. In other words whatever the true value of Δr_{np} is for ^{140}Ce, it is slightly larger for ^{142}Ce. Presumably, a better fit to this data below 6 MeV could be obtained by varying λ_w with energy as was done recently[13] in a microscopic analysis of low energy (10 keV to 10 MeV) neutron cross section data of ^{239}Pu. At low energies the inherent energy dependence of the imaginary part of the JLM potential arising from the Pauli exclusion principle and Reid's hard core interaction is not sufficient to fit the data.

IV. MASS 40 REGION

The absolute neutron total cross section of ^{40}Ca has been measured from 6–57 MeV along with the total neutron cross section difference of ^{44}Ca–^{40}Ca.[2] This $\Delta\sigma_T$ data is not of the same quality as the mass 140 data. Only one difference in cross section was measured and the estimated systematic 33 mb uncertainty of this data is about three times larger than that for the mass 140 region.

The point proton and neutron densities for ^{40}Ca were determined by e^- scattering data and N/Z scaling. With the potentials determined by these densities and λ_v, λ_w chosen, after trial and error, to be 1.01 and 0.77, the solid line fit to the data shown in Fig. 5 was obtained. The agreement between the calculated and measured cross sections is remarkably good.

For ^{44}Ca the point proton densities were determined using e^- scattering difference charge data of ^{44}Ca–^{40}Ca. The neutron densities were chosen in several different ways. First, the neutron density was assumed to be the same as the proton density scaled by N/Z ($\Delta r_{np}=0$). With λ_v, λ_w chosen to be 1.01 and 0.77, the dot-dashed curve of Fig. 6 was obtained for ^{44}Ca–^{40}Ca $\Delta\sigma_T$. Not only is the magnitude of the difference data not reproduced (a recurring problem in attempts to fit this data) but, in addition, the variation of $\Delta\sigma_T$ as a function of energy is not accurately depicted. Varying the parameters λ_v, λ_w improved the fit somewhat, but it became clear that some other changes in the physics beyond a change in the potential strengths were required. There appears to be experimental[14] and theoretical[15] evidence which suggests that while Δr_{np} may be zero for ^{40}Ca, it is not zero for ^{44}Ca but rather is ~0.1 fm. With this as a guide we have also calculated JLM optical potentials for ^{44}Ca with neutron densities chosen such that $\Delta r_{np}=0.13$ fm. This calculation was carried out two ways. The first method assumed that the neutron distribution for ^{44}Ca was the sum of the neutron distribution as calculated for ^{40}Ca plus that due to 4 neutrons in a $1f7/2$ orbital in a Woods-Saxon well.[16] The probability distribution of only the extra 4 neutrons was stretched to yield $\Delta r_{np}=0.13$ fm. The second method started with the smooth neutron ^{44}Ca density implied by N/Z scaling which was in turn stretched radially to achieve the $\Delta r_{np}=0.13$ fm. Both of these calculations predict cross section differences which for all practical purposes are indistinguishable. With λ_v, λ_w assuming the values 1.01 and 0.77, these predictions are represented by the dotted line of Fig. 6. The calculation still does not agree with the data but it has moved in the right direction. The solid curve of Fig. 6 differs from the dotted curve in that λ_v, λ_w were changed to 0.99 and

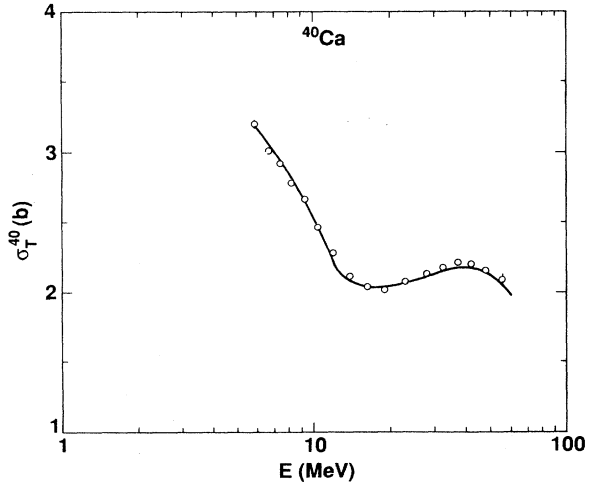

FIG. 5. The measured (circles) ^{40}Ca neutron total cross section as a function of neutron energy (Ref. 2). The solid line is the microscopic optical-model prediction calculation under the assumption that the rms values of proton and neutron densities are equal and with $\lambda_v=1.01$, $\lambda_w=0.77$.

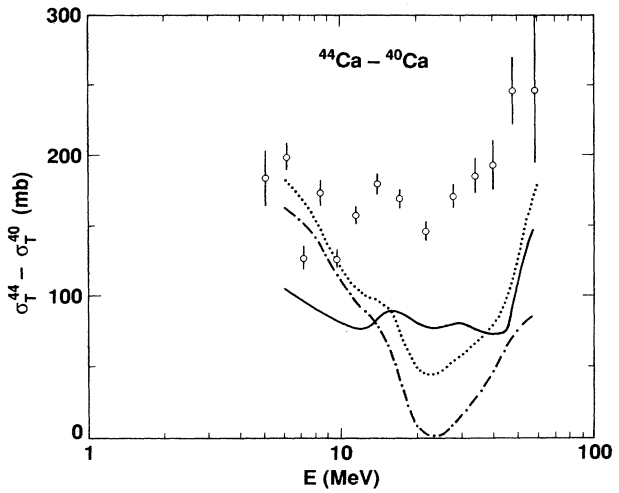

FIG. 6. ^{44}Ca–^{40}Ca $\Delta\sigma_T$ of Ref. 2 as a function of neutron energy along with several predictions of the microscopic model. The dot-dashed curve was obtained by assuming that for ^{44}Ca the neutron density is N/Z times the proton density. The dotted curve was obtained by allowing the ^{44}Ca neutron density rms value to be 0.13 fm larger than that proton rms value but keeping λ_v, λ_w equal to 1.01 and 0.77. Finally, the solid line differs from the dotted curve in that λ_w has been changed to 0.88.

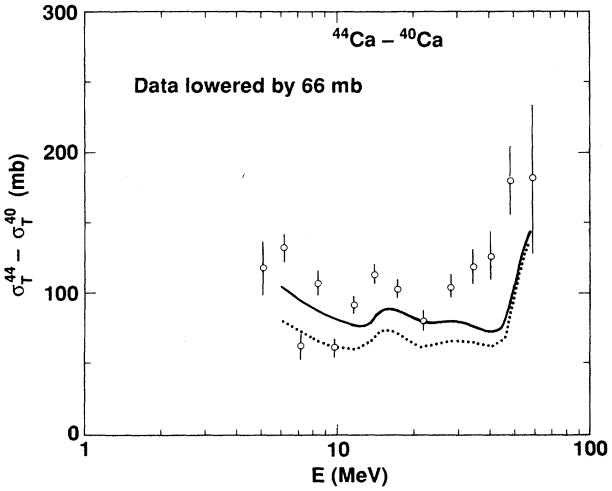

FIG. 7. The solid line of this figure represents the same calculation as the solid line of Fig. 6 for which $\Delta r_{np} = 0.13$ fm. The dotted line differs from the solid line only in that Δr_{np} was chosen to be 0.076 fm. The data has been *lowered* by 66 mb, which is twice the estimated systematic uncertainty of 33 mb, to emphasize that the *shape* of $\Delta\sigma_T$ as a function of neutron energy is represented reasonable well by both curves.

0.88, respectively. The feature we wish to emphasize about the solid curve is that it is a fair representation of the *shape* of the cross section difference as a function of neutron energy. It obviously does not get the magnitude correctly. To emphasize that the shape of the data is being reproduced we have lowered the data by *twice* the estimated 33 mb systematic uncertainty and we have plotted in Fig. 7 this *lowered* data along with predicted cross sections for $\lambda_v = 0.99$, $\lambda_w = 0.88$ and $\Delta r_{np} = 0.13$ fm (solid line) and $\Delta r_{np} = 0.076$ fm (dotted line).

V. CONCLUSION

The results obtained using the JLM microscopic spherical optical model demonstrate that it is a useful tool for understanding the subtle changes which are revealed by a neutron total cross section difference measurement. The fits to the mass 140 $\Delta\sigma_T$ data using the phenomenological potentials[1] and the JLM microscopic model required changes from the ^{140}Ce parameters that were similar. In particular, for the La–Ce and Pr–Ce data the reasonable $\sim A^{1/3}$ changes in the size of the nucleus which led to good phenomenological fits were mirrored in the microscopic model by using proton densities determined from μ^- charge data and N/Z scaling for the neutron densities. For both the microscopic and phenomenological potentials fitting the ^{142}Ce–^{140}Ce data required increasing the strength of the ^{142}Ce imaginary potential by about 10%. Thus both analyses indicate that the addition of two neutrons to the $N = 82$ closed shell of ^{140}Ce requires an increase of the imaginary part of the potential beyond any global change expected from increasing N and A and that this increase is required to an energy of at least 40 MeV. Thus this apparent shell effect persists to a high energy. In addition, making the ^{142}Ce neutron rms radius larger than the proton radius for the JLM optical potentials appears to be analogous to the increased diffuseness required ^{142}Ce in the phenomenological potentials[1]

For the fits to the ^{44}Ca–^{40}Ca $\Delta\sigma_T$ data using either the JLM or the phenomenological potentials,[2] changes similar to those required for the ^{142}Ce–^{140}Ce difference data were made. Again, neutrons are being added to a closed neutron shell nucleus, and the imaginary parts of both potentials were increased. In addition, for the JLM potential Δr_{np} was chosen to be greater than zero and in the phenomenological potential[2] additional diffuseness was introduced into the ^{44}Ca nucleus. The phenomenological analysis also required an increase in strength of the $(N-Z)/A$ term of the ^{44}Ca potential in order to fit the ^{44}Ca–^{40}Ca difference data. A change of this nature was not made in the JLM potential.

The very important advantage of the microscopic potential lies in the possibility of pinpointing more accurately where changes are required to improve the fits to the data, e.g. in the neutron rms radius. Furthermore, the goal of any analysis is to extract physics from the data and the smaller number of free parameters of the microscopic optical model gives greater confidence in this regard.

This work was performed under the auspices of the U.S. Department of Energy by the Lawrence Livermore National Laboratory under Contract No. W-7405-ENG-48.

[1] H. S. Camarda, T. W. Phillips, and R. M. White, Phys. Rev. C **29**, 2106 (1984).
[2] H. S. Camarda, T. W. Phillips, and R. M. White, Phys. Rev. C **34**, 810 (1986).
[3] J. P. Jeukenne, A. Lejeune, and C. Mahaux, Phys. Rep. **25C**, 83 (1976).
[4] J. P. Jeukenne, A. Lejeune, and C. Mahaux, Phys. Rev. C **16**, 80 (1977).
[5] A. Lejeune, Phys. Rev. C **21**, 1107 (1980).
[6] S. Mellema, R. W. Finlay, F. S. Dietrich, and F. Petrovich, Phys. Rev. C **28**, 2267 (1983).
[7] L. F. Hansen, F. S. Dietrich, B. A. Pohl, C. H. Poppe, and C. Wong, Phys. Rev. C **31**, 111 (1985).
[8] N. Olsson, B. Trostell, E. Ramstrom, B. Holmqvist, and F. S. Dietrich, Nucl. Phys. **A472**, 237 (1987).
[9] J. W. Negele and K. Yazaki, Phys. Rev. Lett. **47**, 71 (1981).
[10] S. Fantoni, B. L. Friman, and V. R. Pandharipande, Phys. Lett. **104B**, 89 (1981).
[11] C. W. DeJager, H. De Vries, and C. De Vries, At. Data Nucl. Data Table **14**, 79 (1974).
[12] R. Engfer, H. Schneuwly, J. L. Vuilleumier, H. K. Walter, and A. Zehnder, At. Data Nucl. Data Tables **14**, 509 (1974).
[13] Ch. Lagrange, D. G. Madland, and M. Girod, Phys. Rev. C **33**, 1616 (1986).
[14] R. H. McCamis *et al.*, Phys. Rev. C **33**, 1624 (1986).
[15] J. Dechargé and D. Gogny, Phys. Rev. C **21**, 1568 (1980).
[16] K. Bear and P. E. Hodgson, J. Phys. G **4**, L287 (1978).